



Numerical investigation of terahertz wave driven electron acceleration generated from gas jet

Sz. Turnár^{1,3} · B. Sarkadi¹ · S. W. Jolly² · J. Hebling^{1,4} · Z. Tibai¹

Received: 1 June 2023 / Accepted: 2 December 2023 / Published online: 8 January 2024
© The Author(s) 2024

Abstract

We have investigated the dependence of the acceleration efficiency for three different proposed direct terahertz wave driven electron accelerator setups, including ionization in a gas jet source. We have numerically simulated and optimized the ionization processes using Particle-In-Cell code (EPOCH) and pointed out its crucial effect on the accelerating mechanism. Supposing two single-cycle terahertz driving pulses with 1 mJ energy per pulse we characterized the different accelerator arrangements. The main properties of the predicted electron beams with the average kinetic energy of 27 keV can be adapted to the requirements of different applications in the fC-pC charge range.

1 Introduction

Terahertz radiation sources with high field strength remained relatively unexplored by researchers for a long time, but the field is currently undergoing significant advancements due to a diverse range of potential applications and improvements in driving laser technology. The advantage of the THz pulse-based particle manipulator devices compared to radio frequency is that their smaller size enables simplicity and greater compactness, while their picosecond range pulse length enables interaction with the entire electron bunch and can ensure proper synchronization. However, the required energy level of the THz pulses to achieve efficient electron acceleration has been unavailable during the last decades and the electron manipulation techniques and devices powered by THz pulses were also in their infancy. Nowadays, thanks to technological development [1] and new ideas [2], several THz sources with up to a few 100 kV/cm [3], or even MV/cm field strength have been experimentally demonstrated [4,

5]. Such newly proposed sources have already made possible the realization of both electron acceleration [6, 7] and electron characterization [8] arrangements based on THz pulses.

Multiphoton ionization with intense ultrashort laser pulses in Krypton gas has also been investigated numerically [9] and experimentally [10]. In contrast to the electron source generated by the well-proven photoemission technique, in our previous work we assumed electrons created by ionization from optical lasers in Krypton gas jet as the electron source [11, 12] without considering the details of this source. The gas jet allows the relatively easy manipulation of the size and charge of the electron bunch, it also enables more technical elements to be easily implemented in the experimental setup, such as applying more accelerator pulses compared to an electron gun. In this paper, we further investigate our earlier proposed setup [11], wherein counter-propagating THz-pulses were used to directly accelerate electrons from a gas jet, while the ionization was carried out by intense and ultrashort optical laser pulse. Now we show that during the ionization processes the continuously generated particles perceive different accelerating fields in time and space, so the arising time and the distribution of the electrons in space and time have a decisive influence on the acceleration efficiency. Using EPOCH particle-in-cell (PIC) [13] code we simulated and optimized the main parameters of the ionization process, such as the beam waist and the initial charge densities to achieve the highest kinetic energy and the smallest energy spread after the acceleration.

✉ Sz. Turnár
turnarszabolcs@fizika.ttk.pte.hu

¹ Institute of Physics, University of Pécs, 7624 Pécs, Hungary

² Service OPERA-Photonique, Université Libre de Bruxelles (ULB), Brussels, Belgium

³ HUN-REN-PTE High-Field Terahertz Research Group, 7624 Pécs, Hungary

⁴ Szentágothai Research Centre, University of Pécs, 7624 Pécs, Hungary

2 Details of the calculation

The spatiotemporal modelling of direct acceleration with high-field terahertz pulses has been provided via simulations in our previous work [14], whereby two identical mostly counter-propagating single-cycle THz pulses produce a standing wave and accelerate an electron, which is assumed to be at the zero-crossing point of the electric field of the THz pulses. The model has three relevant features: (i) besides the transversal field it includes the modelling of the longitudinal field, which is necessary due to the tight focusing; (ii) it calculates with the Poisson spectral amplitude shape, which was a result of the duration of the pulse being reduced to a single cycle; and (iii) describing the propagation of the accelerator pulse, its chromatic nature was taken into account that was also significant because of the single-cycle duration [15–17].

The model utilizes a constant number of macroparticles, which is consistent with 10 fC initial bunch charge in the case of 1:1 macroparticle-electron ratio. The charge of the bunches was modified by changing the number of the electrons per macroparticle. The field of a tightly focused electromagnetic wave, which is responsible for the acceleration of the particles and linearly polarized in the z' direction at frequency ω , is the following:

$$\vec{E}(x', z', \omega) = E_0 \frac{w_0}{w(x')} e^{-\frac{z'^2}{w(x')^2}} e^{i\psi} \times \left[\hat{z}' - \frac{2iz'}{k} \left(\frac{1}{w(x')^2} + \frac{k}{2iR(x')} \right) \hat{x}' \right] \quad (1)$$

$$\psi(x') = kx' - \omega t + \frac{kz'^2}{2R(x')} - \eta(x') + \phi_0, \quad (2)$$

where $x' = x \cos \alpha$ and $z' = z \cos \alpha$ are the propagation and polarization direction of the THz pulses after the tilting at an angle α , respectively. The $w(x') = w_0 \sqrt{1 + \left(\frac{x'}{z_R}\right)^2}$ is the evolving beam radius, $R(x') = x' \left[1 + \left(\frac{x'}{z_R}\right)^2 \right]$ is the radius of the curvature, $\eta(x') = \arctan\left(\frac{x'}{z_R}\right)$ is the Gouy phase along the propagation direction (x'), and ϕ_0 is the carrier-envelope-phase (CEP). The beam waist is w_0 with the Rayleigh range $z_R = \frac{\omega w_0^2}{2c}$ and $k = \frac{\omega}{c}$.

The peak electric field of the slightly tilted accelerator pulses with 0.3 THz central frequency was 5.21 MV/cm. We consider the electric field as a sine function. The initial value of the tilting angle of the THz pulses was set to 4° , while the relative carrier envelope phase was zero. Using Eq. (1) we further improved our numerical simulations to create more realistic model to generate and accelerate electron bunches.

We simulated the generation of the electron bunches and in addition optimized the parameters of the investigated accelerator setups. Particle-in-Cell code (EPOCH) was used to simulate the ionization of the electron bunches, while the General Particle Tracer (GPT) software [18] was applied to simulate the acceleration of the previously generated particles.

We have examined three different ionization arrangements. Our proposed setups, which are shown in Fig. 1a–c, include the process of the electron bunch ionization by femtosecond laser pulse(s) and afterwards the acceleration of the generated electron bunches by mostly counterpropagating THz pulses. For the electron source we assumed a Krypton gas jet with a nozzle diameter of 100 μm . The particle number density was $1.04 \times 10^{20} \frac{1}{\text{m}^3}$. The Krypton gas is supposed to be ionized by an Yb:KGW laser (wavelength = 1030 nm, FWHM = 170 fs). This laser can be the same as the pump for the generation of the (accelerator) THz pulses [19]. The propagation direction of the ionizing laser pulse(s) is perpendicular to the propagation direction of the THz pulses. In case I (Fig. 1a) the propagation direction of the ionizing laser pulse is the same as the acceleration direction of the THz field. In case II (Fig. 1b) the propagation direction of the ionizing laser pulse opposed to the acceleration direction of the THz field. In case III (Fig. 1c) two counterpropagating ionizing laser pulses generate the electrons. The schematic views of the spatial distributions of the ionized electron bunches predicted for the different ionization setups are shown in Fig. 1d–g.

By modifying the beam waist of the ionizing laser pulse(s), it is possible to control the transversal size of the generated electron bunches. Furthermore, the initial bunch charge in addition to the initial number density of the gas could also be controlled by the intensity of the ionizing laser pulse(s). At constant bunch charges, by changing the initial volume of the ionized region, the charge densities of the electron beams are also different in case of the various acceleration arrangements. In case I and case II the longitudinal length of the ionized region could only be controlled by the diameter of the nozzle. Typically, it is greater than 0.1 mm [20, 21]. However, in case III the length of the generated electron bunch in the propagation direction of the ionizing laser pulses can also be controlled by the ionizing pulse duration. Using two femtosecond laser pulses with around 49 μJ energy the ionized electron bunch shape is close to a sphere with 20 μm FWHM bunch diameter and with around 10 fC bunch charge. Using one ionizing pulse the electron bunch generation with 10 μm (FWHM) transversal bunch size and with charge of 10 fC requires around 38 μJ energy. While in case of the 20 μm (FWHM) initial transversal bunch size and around 1 pC initial bunch charge the energy of the ionizing laser pulse is 204 μJ .

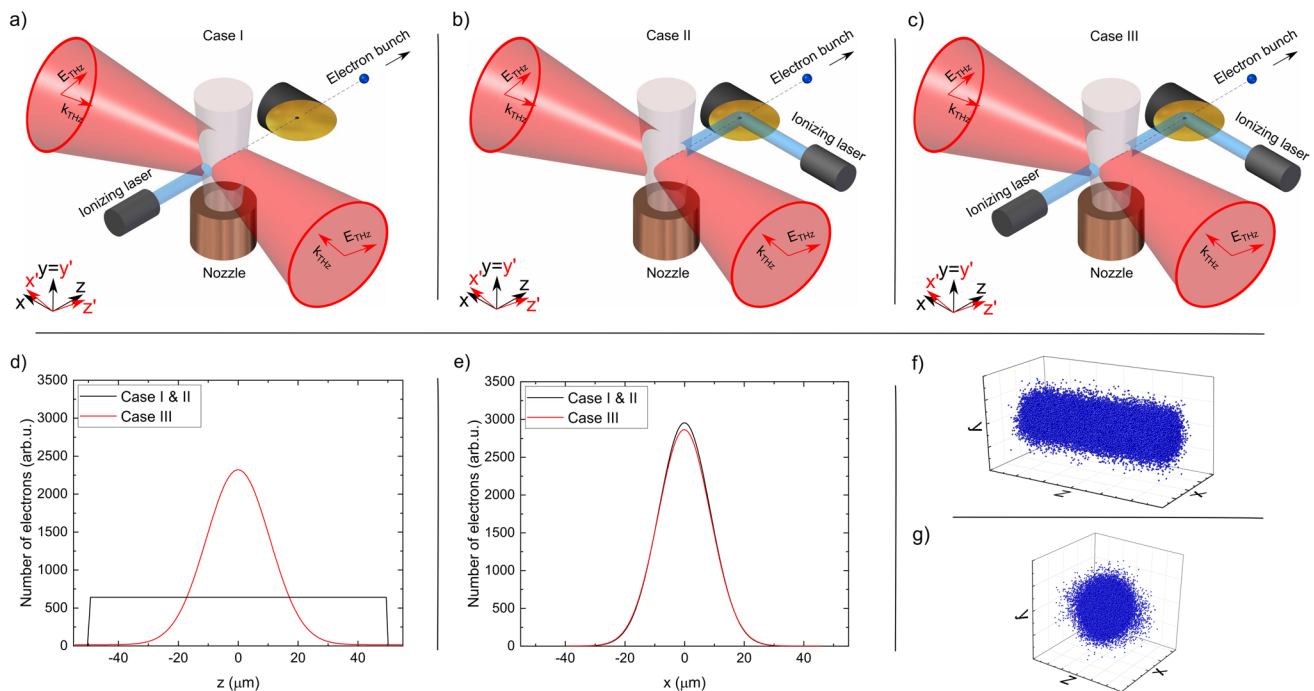


Fig. 1 The schematic view of the ionization and acceleration methods. **a** The propagation direction of the ionizing laser pulse is the same as the acceleration direction of the THz pulses (case I). **b** The propagation direction of the ionizing laser pulse opposed to the acceleration direction of the THz pulses (case II). **c** Two counterpropagating ionizing laser pulses generate the electrons (case III). **d** The spatial distributions in the direction of the acceleration of the ionized

electron bunches in all cases (black line: case I and case II, red line: case III). **e** The spatial distributions in the transversal x -direction of the ionized electrons in all cases (black line: case I and case II, red line: case III). The electron bunches have rotation symmetry in the x - y plane. The generated initial electron bunches in 3 dimensions **f** with the case I and case II and **g** with case III setup

3 Results

We have examined the efficiency of the electron bunch acceleration with respect to the energy spectra in the case of the optimal settings for electron acceleration obtained in ref. [11]. It is assumed that the electron in the middle of the interaction area is born at the zero-crossing point of the electric field of the THz pulses. The results can be seen in Fig. 2a. This is the most optimal case (MOC) with respect to the achievable kinetic energy. Using 1 mJ energy per THz pulse we have investigated the electron bunch acceleration with two different initial bunch diameters ($\text{FWHM}_{x,y} = 10 \mu\text{m}$, $\text{FWHM}_{x,y} = 20 \mu\text{m}$) in the transversal directions and with many initial bunch charges on the interval of 1–6000 fC.

In the numerical simulations of the particle acceleration, we have also investigated two different cases with regards to the generation time of the particles. The first is the “prompt” case, when the shape of the initial electron bunches was determined by simulating the ionizing processes with the PIC code, but the birth time of all the electrons corresponds with the MOC electron generation time. The second case is the “realistic” case, when along with the other properties of the particles such as coordinates and velocities, the birth time of the electrons was

also determined by the PIC simulations depending on the ionizing laser parameters, while the central electron was still born at the MOC time. The calculated energy of a single electron, which is around 27 keV, is shown by the magenta dash-dotted line. We used it as a reference value. Thereafter, we have compared the results of the acceleration of different initial bunches generated by case I-III ionizing setups with $10 \mu\text{m}$ (FWHM) transversal size. In these simulations, the charge of the macroparticle bunches was set to 1 fC, in order that the space charge be negligible. So, the differences between the obtained energy spectra after the acceleration are caused by the effects of the different ionizing methods. By examining the particles generated during the previously described ionization and acceleration processes I-II it could be seen that using the simulation parameters of the MOC after the particle-electric field interactions the electron bunches could be accelerated up to the reference 27 keV kinetic energy. In the case III ionization and acceleration process only the prompt scenario gives around 27 keV average kinetic energy, while using the realistic setup the mean energy of the bunch is only around 24.5 keV. The deviation from the reference energy in the prompt cases, since all electrons are born at the time used for the MOC, is therefore due to their initial

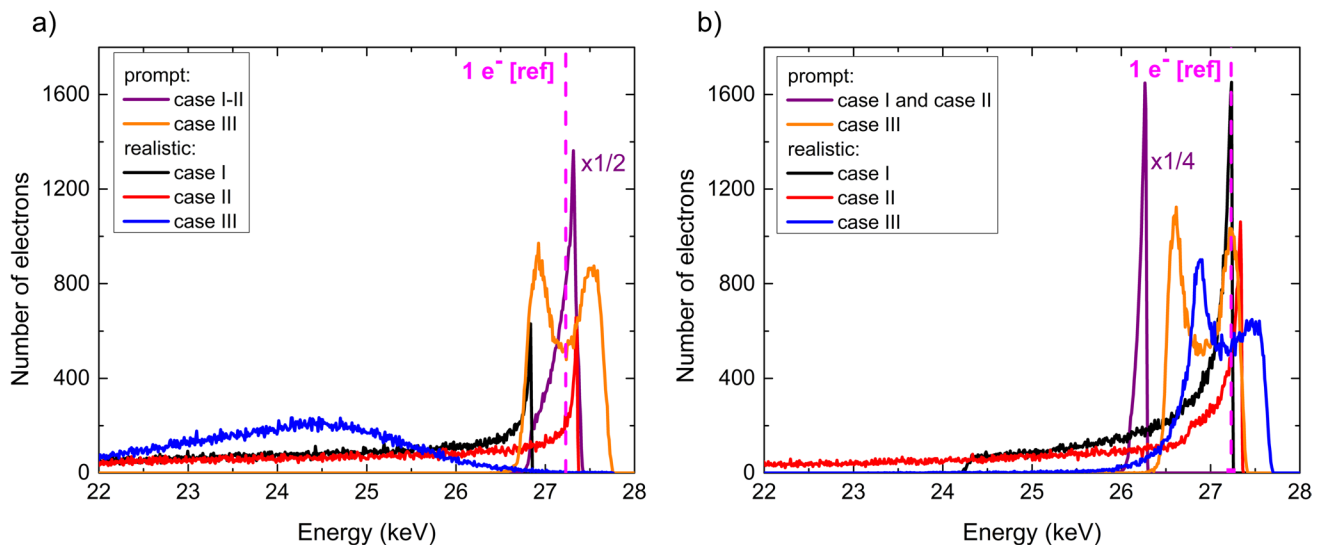


Fig. 2 The energy spectra of the electron bunches after the acceleration **a** in case of the time synchronization with the MOC and **b** in case of the realistic time synchronization, which was optimized to

spatial positions. In the realistic case, the deviations are due to their initial space and time values. For the realistic case III, the much larger deviation is due to the relatively major difference between the generation time of the electrons compared to the MOC. In conclusion, the role of the realistic (time dependent) electron generation using different ionization procedure is essential in the numerical simulations.

Adjusting the electron bunch generation and the THz pulse synchronization we further optimized the acceleration ensuring that the energy spectrum was as narrow as possible, and the number of the efficiently accelerated electrons was the greatest. Figure 2b shows these results.

It can be stated that in the case of the acceleration of the electron bunches generated by different ionizing setups, a good starting point can be the time synchronization determined by the MOC electron acceleration. However, to increase the acceleration efficiency and narrow the energy spectrum, a new time synchronization is required in each case. Our results show that in each case the electron bunches could be accelerated to around 27 keV average kinetic energy once optimized. It can also be seen that by assuming the case I prompt setup the number of the efficiently accelerated electrons is higher by a factor of 4 compared to the other cases. Our results also show that the energy spectra of the accelerated electron bunches strongly depend on the ionizing setups.

Applying the optimized temporal synchronizations, we extended our realistic (time-dependent) calculations to the case of electron bunches with different initial charges. We have investigated the bunches produced by different

get the narrowest energy spectra and the greatest number of the efficiently accelerated electrons

ionization processes after the acceleration at the time of 100 ps (it means ~ 10 mm propagation distance from the gas jet). Figure 3 shows the energy spectra of the electron bunches with different bunch charges and with a-d 10 μm and e-h 20 μm transversal bunch sizes (FWHM), respectively. The initial charge of the macroparticle bunches was changed in the range of 10–1000 fC. The initial charges are fixed values, so the charge densities of the bunches generated by case I and case II are the same, while the initial densities generated by the case III are greater in each case. The numerical simulations show that by applying the case I–III ionization and accelerator setups there is a considerable difference between the energy spectra of the accelerated electron bunches.

Based on the results it can be said that, in the case of the 10 fC initial electron bunch charge in case I and case II setups the smaller initial size (FWHM = 10 μm) is more advantageous, as more electrons could be accelerated to higher energies, than in the 20 μm (FWHM) case. In case I by increasing the initial bunch charge to a few hundreds of femtocoulomb, the advantage of the smaller initial bunch size remains. The width of the spectra is around the same in case of the electron bunches with 10 and 20 μm initial bunch diameters, but the difference between the number of the electrons with average kinetic energy is around 30% in favour of the case 10 μm (FWHM) initial transversal size. In case II by increasing the initial bunch charge the advantage of the smaller size gradually disappears with respect to the number of the efficiently accelerated electrons. The case III setup is barely sensitive to the initial bunch size in the investigated charge range. Moreover, by making allowance

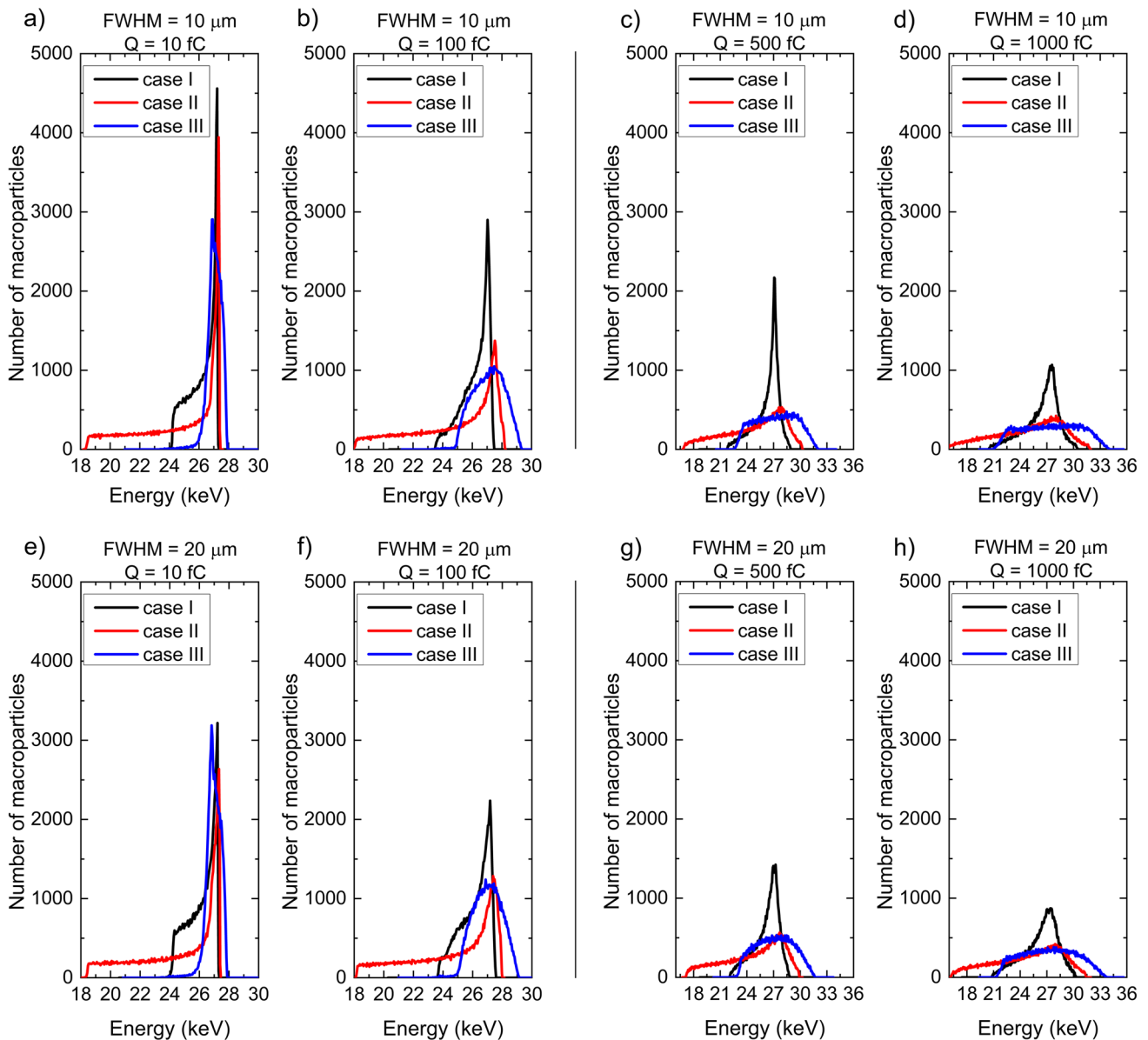


Fig. 3 The energy spectra of the accelerated electron bunches with the initial charge of 10, 100, 500, and 1000 fC, which were generated by case I-III ionizing methods with **a–d** 10 μm and **e–h** 20 μm initial

transversal bunch sizes (FWHM), respectively. The achievable kinetic energies and thereby the range of the *x* axes are different in case of a smaller (≤ 100 fC) and higher (≥ 500 fC) bunch charges

for the number of the efficiently accelerated electrons on the swept charge interval (10–1000 fC) the greater initial bunch size has an advantage.

According to the numerical simulations, the larger the initial bunch charge is, the larger the width of the energy spectra. The observable broadening is the most considerable when the initial electron bunches generated by the case II arrangement. In conclusion, if the given application requires a narrow energy spectrum ($\Delta E < 3\%$ (rms)) and a relatively small bunch charge ($Q < \text{few tens of fC}$), then

considering the conditions defined by us in this paper, the case III arrangement must be applied for the acceleration. In the case of the initial bunch charge of a few hundreds of femtocoulombs, the narrowest ($3\% < \Delta E < 7\%$ (rms)) spectrum is predicted by the case I arrangement. The simulation results of the case I give the narrowest energy spectra in the charge range of a few pC (1–6 pC) as well, their energy spreads are between 7 and 17% (rms).

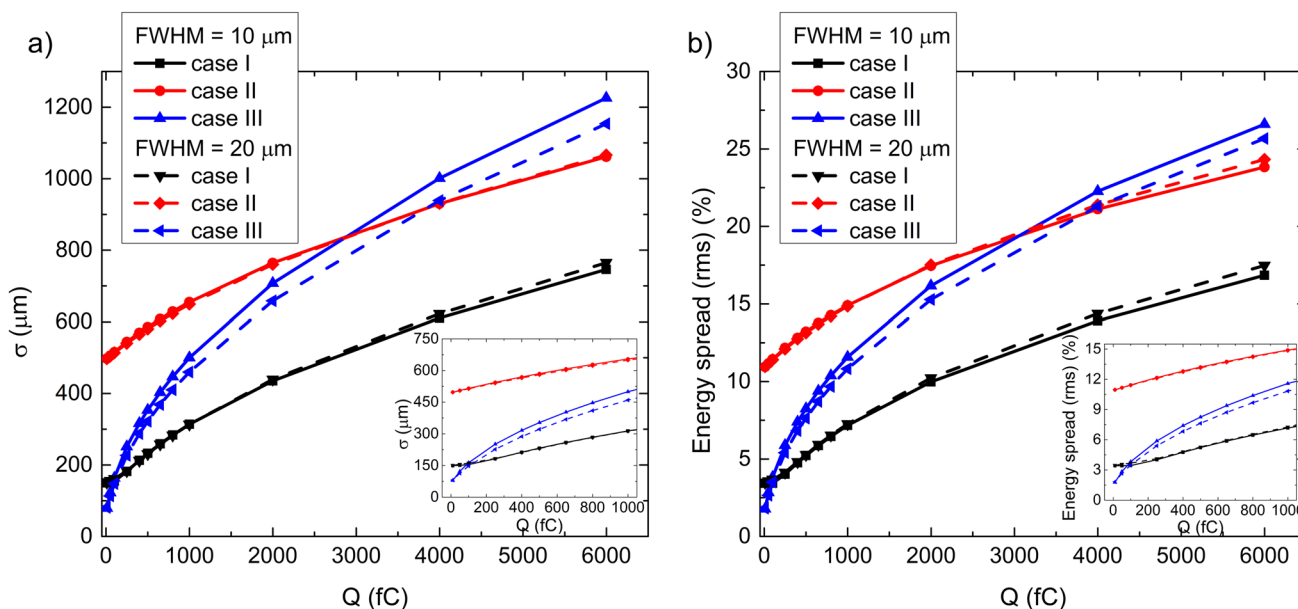


Fig. 4 **a** The length and **b** the energy spread of the accelerated electron bunches, which were generated by case I-III setups in the charge interval of 10–6000 fC with 10 μm and 20 μm initial bunch sizes

Table 1 Classification of the suggested setups by different initial bunch charges and the predicted results

Charge [fC]	Suggested setup	Optimal initial transverse size [μm] ^a	Optimal initial Longitudinal size [μm] ^b	Final energy spread (rms) [%]	Final standard deviation (rms) [μm]
≤ 10	Case III	10–20	10–20	~ 1.5	80
100	Case III	20	20	~ 3.5	147
500	Case I	10–20	100	~ 5.2	230
1000	Case I	10–20	100	~ 7.3	315
1000–6000	Case I	10–20	100	$\sim 7.3 - 17.0$	315–750

^aBy supposing Case I and Case III the optimal initial transverse size is in FWHM

^bBy supposing Case I the optimal initial longitudinal size means the total length of the bunch in the acceleration direction. In Case III it means the size in FWHM. If a range is specified, experiments can be conducted with any initial size in the interval by providing almost the same result

4 Properties of the accelerated electron bunches

To be able to compare the electron bunches more precisely we quantified the main properties of the efficiently accelerated electrons. We determined the length of the accelerated electron bunches and its energy spreads in rms, respectively. The results are shown in Fig. 4 in case of the 10 μm and 20 μm initial transversal bunch sizes (and marked with solid and dashed lines), respectively. The calculations were extended to all investigated realistic ionizing and accelerating methods. Assuming smaller initial bunch charges ($Q < \text{few hundreds of fC}$), the distances between the solid and dashed lines, so the differences between the longitudinal length of the accelerated bunches with different initial transversal sizes are almost

negligible. If the charge of a bunch is increased, the differences increase continuously. Increasing the transversal size results in larger improvement in both the bunch length and the energy spread in the case of setup III. This is expected, since in this case the charge density is the largest for a given bunch. Assuming the case III setup the investigated greater bunch size is more beneficial compared it with the smaller bunch size. Generating electron bunches with case III setup and with an initial charge of 6000 fC the difference between the length of the bunches with different transversal sizes is $\sim 7\%$.

In the accelerator setup of case I and case II and assuming a few pC bunch charges, the examined smaller bunch size is more advantageous. Applying case II setup and supposing charges on the entire range of the investigated interval, the length of the bunch in the longitudinal direction after the

acceleration is constantly greater than in case I, the differences between the longitudinal sizes are between 330 and 150% (By increasing the charge of the bunch, the difference between the longitudinal length decreases). Moreover, based on the results, it can be stated that up to an initial charge of 1–2 pC the length of the accelerated electron bunch produced by case II setup is longer after the acceleration, as the bunch length in case III setup. On the other hand, the difference in bunch length between the two cases when the charge is further increased disappears and eventually changes sign, i.e., the length of the bunch produced with case III setup will be greater after the acceleration than in case II.

In conclusion, we have determined that below about 100 fC bunch charge, the ionization and acceleration by the case III setup is the most advantageous considering the main parameters of the electron bunch, such as the longitudinal length and the energy spread. At larger bunch charges the case I setup is optimal. For easier transparency, we have summarized the results in Table 1.

5 Conclusion

We have shown that assuming different ionizing arrangements, and two roughly counter-propagating THz pulses with 1 mJ energy per pulse, by changing the parameters of the ionizing laser(s), electron bunches with different properties can be produced. We have also examined the effect of both the prompt and realistic bunch generation on the acceleration efficiency. After accelerating the electron bunches produced by different ionization techniques in the investigated fC-pC initial charge range with THz pulses, different electron beams are predicted. Our numerical simulations also show that assuming a few tens of fC initial bunch charge, the most optimal case in terms of the longitudinal size and the energy distribution of the bunch is when two counterpropagating ionizing pulses, which propagate perpendicular to the accelerator pulses, generate the electrons from the gas jet source. Increasing the charge further up to a few pC, the optimal setup is when the propagation direction of the ionizing laser pulse is the same as the acceleration direction of the accelerator (THz) pulses. We have also stated that if the shape of the initial electron bunch must be matched to different initial shapes, using two counterpropagating ionizing laser pulses and setting properly their main parameters along with the diameter of the nozzle is the best method to control that.

Acknowledgements The project has been supported by the National Research, Development and Innovation Office (2018-1.2.1-NKP-2018-00010, TKP2021-EGA-17). Supported by the ÚNKP-22-4 New National Excellence Program of the Ministry for Culture and Innovation from the source of the National Research, Development and

Innovation Fund (Turnár Szabolcs). Zoltán Tibai would like to thank the support of the János Bolyai Research Scholarship of the Hungarian Academy of Science. S.W.J. has received funding from the European Union's Horizon 2020 research and innovation programme under the Marie Skłodowska-Curie Grant Agreement No. 801505. The EPOCH code used in this work was in part funded by the UK EPSRC grants EP/G054950/1, EP/G056803/1, EP/G055165/1, EP/M022463/1 and EP/P02212X/1. Supported by TWAC is funded by the EIC Pathfinder Open 2021 of the Horizon Europe program under grant agreement 101046504.

Author contributions SzT: investigation of acceleration, wrote the main manuscript, prepared figures. BS: investigation of ionization, prepared figures, SWJ: methodology, writing—review and editing. JH: methodology, writing—review and editing. ZT: methodology, writing—review and editing, supervision. All authors reviewed the manuscript.

Funding Open access funding provided by University of Pécs.

Data availability The corresponding authors can provide the datasets generated and analyzed in the current study upon reasonable request.

Declarations

Conflict interest The authors declare no competing interests.

Open Access This article is licensed under a Creative Commons Attribution 4.0 International License, which permits use, sharing, adaptation, distribution and reproduction in any medium or format, as long as you give appropriate credit to the original author(s) and the source, provide a link to the Creative Commons licence, and indicate if changes were made. The images or other third party material in this article are included in the article's Creative Commons licence, unless indicated otherwise in a credit line to the material. If material is not included in the article's Creative Commons licence and your intended use is not permitted by statutory regulation or exceeds the permitted use, you will need to obtain permission directly from the copyright holder. To view a copy of this licence, visit <http://creativecommons.org/licenses/by/4.0/>.

References

1. J.A. Fülöp, G. Polónyi, B. Monoszlai, G. Andriukaitis, T. Balciunas, A. Pugzlys, G. Arthur, A. Baltuska, J. Hebling, *Optica* **3**, 1075 (2016)
2. B.K. Ofori-Okai, P. Sivarajah, W.R. Huang, K.A. Nelson, *Opt. Express* **24**, 5057 (2016)
3. T. Seifert, S. Jaiswal, M. Sajadi, G. Jakob, S. Winnerl, M. Wolf, M. Kläui, T. Kampfrath, *Appl. Phys. Lett.* **110**, 252402 (2017)
4. M. Shalaby, C.P. Hauri, *Nat. Commun.* **6**, 5976 (2015)
5. B. Zhang, Z. Ma, J. Ma, X. Wu, C. Ouyang, D. Kong, T. Hong, X. Wang, P. Yang, L. Chen, Y. Li, J. Zhang, *Laser Photon Rev* **15**, 2000295 (2021)
6. A. Fallahi, M. Fakhari, A. Yahaghi, M. Arrieta, F.X. Kärtner, *Phys Rev Acc Beams* **19**, 081302 (2016)
7. E.A. Nanni, W.R. Huang, K.-H. Hong, K. Ravi, A. Fallahi, G. Moriena, R. Dwayne Miller, F.X. Kärtner, *Nat. Commun.* **6**, 8486 (2015)
8. R.K. Li, M.C. Hoffmann, E.A. Nanni, S.H. Glenzer, M.E. Kozina, A.M. Lindenberg, B.K. Ofori-Okai, A.H. Reid, X. Shen, S.P. Weathersby, J. Yang, M. Zajac, X.J. Wang, *Phys. Rev. Acc. Beams* **22**, 012803 (2019)

9. I. Azzouz, Nucl. Instrum. Methods Phys. Res., Sect. B **205**, 337 (2003)
10. H. Maeda, M. Dammasch, U. Eichmann, W. Sandner, A. Becker, F. Faisal, Phys. Rev. A **62**, 035402 (2000)
11. Z. Tibai, M. Unferdorben, S. Turnár, A. Sharma, J. Fülöp, G. Almási, J. Hebling, Journal of Physics B: Atomic, Molecular and Optical Physics **51**, 134004 (2018)
12. S. Turnár, J. Hebling, J. Fülöp, G. Tóth, G. Almási, Z. Tibai, Appl. Phys. B **127**, 1 (2021)
13. T.D. Arber, K. Bennett, C.S. Brady, A. Lawrence-Douglas, M.G. Ramsay, N.J. Sircombe, P. Gillies, R.G. Evans, H. Schmitz, A.R. Bell, C.P. Ridgers, Plasma Phys. Controlled Fusion **57**, 113001 (2015)
14. Z. Tibai, S. Turnár, G. Tóth, J. Hebling, S.W. Jolly, Opt. Express **30**, 32861 (2022)
15. A.P. Miguel, J. Opt. Soc. Am. B **16**, 1468 (1999)
16. M.A. Porras, Phys. Rev. E **58**, 1086 (1998)
17. M.A. Porras, Phys. Rev. E **65**, 026606 (2002)
18. S.B. Van Der Geer, O.J. Luiten, M.J. De Loos, G. Pöplau, and U. van Rienen: Institute of Physics Conference Series, No.175, p. 101. (2005). <https://www.pulsar.nl/gpt/>
19. G. Tóth, L. Pálfalvi, S. Turnár, Z. Tibai, G. Almási, J. Hebling, Chin. Opt. Lett. **19**, 111902 (2021)
20. J. Holburg, M. Müller, K. Mann, Opt. Express **29**, 6620 (2021)
21. J. Jauberteau, I. Jauberteau, J. Aubreton, Int. J. Mass Spectrom. **235**, 179 (2004)

Publisher's Note Springer Nature remains neutral with regard to jurisdictional claims in published maps and institutional affiliations.